

# MOBSTER - IV. Detection of a new magnetic B-type star from follow-up spectropolarimetric observations of photometrically selected candidates<sup>★</sup>

A. David-Uraz,<sup>1†</sup> M. E. Shultz,<sup>1</sup> V. Petit,<sup>1</sup> D. M. Bowman,<sup>2</sup> C. Erba,<sup>1</sup>  
R. A. Fine,<sup>1</sup> C. Neiner,<sup>3</sup> H. Pablo,<sup>4</sup> J. Sikora,<sup>5</sup> A. ud-Doula<sup>6</sup>, and G. A. Wade<sup>7</sup>

<sup>1</sup>*Department of Physics and Astronomy, University of Delaware, Newark, DE 19716, USA*

<sup>2</sup>*Institute of Astronomy, KU Leuven, Celestijnenlaan 200D, B-3001 Leuven, Belgium*

<sup>3</sup>*LESIA, Paris Observatory, PSL University, CNRS, Sorbonne University, Université de Paris, 5 place Jules Janssen, 92195 Meudon, France*

<sup>4</sup>*American Association of Variable Star Observers, 49 Bay State Rd., Cambridge, MA, 02138, USA*

<sup>5</sup>*Department of Physics and Astronomy, Bishop's University, Sherbrooke, Québec, Canada, J1M 1Z7*

<sup>6</sup>*Penn State Scranton, 120 Ridge View Drive, Dunmore, PA 18512, USA*

<sup>7</sup>*Department of Physics and Space Physics, Royal Military College of Canada, PO Box 17000 Kingston, ON K7K 7B4, Canada*

Accepted XXX. Received YYY; in original form 2020 April 21

## ABSTRACT

In this paper, we present results from the spectropolarimetric follow-up of photometrically selected candidate magnetic B stars from the MOBSTER project. Out of four observed targets, one (HD 38170) is found to host a detectable surface magnetic field, with a maximum longitudinal field measurement of  $105 \pm 14$  G. This star is chemically peculiar and classified as an  $\alpha^2$  CVn variable. Its detection validates the use of *TESS* to perform a photometric selection of magnetic candidates. Furthermore, upper limits are derived for the remaining three stars, and we report the discovery of a previously unknown spectroscopic binary system, HD 25709. Finally, we use our non-detections as case studies to further inform the criteria to be used for the selection of a larger sample of stars to be followed up using high-resolution spectropolarimetry.

**Key words:** stars: early-type – stars: magnetic field – stars: rotation – techniques: photometric – techniques: spectroscopic – techniques: polarimetric

## 1 INTRODUCTION

It has been well established by large spectropolarimetric surveys that there exists a distinct population of magnetic OBA stars, with an incidence of roughly 10 per cent (e.g. Donati & Landstreet 2009; Wade et al. 2016a; Grunhut et al. 2017; Schöller et al. 2017; Sikora et al. 2019a). A key feature of this population is a lack of correlation between magnetic and stellar properties (Shultz et al. 2019b), and there is still much debate surrounding the formation mechanism of these magnetic fields (e.g. Schneider et al. 2016; Villebrun et al. 2019). The evolution of the magnetic field is also poorly constrained, although there are preliminary indications that the usual assumption of flux conservation might not hold at higher masses (Landstreet et al. 2007, 2008; Fossati et al. 2016; Shultz et al. 2019b).

The main hindrance to answering these fundamental questions resides in small number statistics, especially for the more massive magnetic stars: to date, there are only 11 known magnetic O-type stars (Petit et al. 2013; Fossati et al. 2016) and less than 100 known magnetic early B-type stars (Shultz et al. 2018b). Given the large cost of spectropolarimetry, we propose that the potential of blind surveys to significantly increase this sample has effectively reached its limit. Targeted efforts relying on indirect magnetic diagnostics<sup>1</sup> to build up candidate lists yield much higher detection rates (Buysschaert et al. 2018). In particular, high-precision photometric missions such as the Transiting Exoplanet Sur-

<sup>1</sup> Such diagnostics include  $H\alpha$  or Brackett line emission (e.g. Walborn 1974; Eikenberry et al. 2014), rotationally modulated photometry (e.g. Munoz et al. 2020; Bagnulo et al. 2020), chemical peculiarities (Babcock 1958) and the presence of specific spectral features such as the CIII/NIII emission complex in the optical spectra of Of?p spectral class stars (Walborn 1972; Grunhut et al. 2017).

<sup>★</sup> Based on observations collected at the Canada-France-Hawaii Telescope (CFHT).

† E-mail: adu@udel.edu

vey Satellite (*TESS*; Ricker et al. 2015) play an instrumental role in identifying such magnetic candidates. The MOBSTER (Magnetic OB[A] Stars with *TESS*: probing their Evolutionary and Rotational properties; David-Uraz et al. 2019) Collaboration was formed to leverage *TESS* for this specific purpose.

This paper presents the first new magnetic detection achieved by the MOBSTER Collaboration and establishes the bases for its ongoing efforts to perform targeted spectropolarimetric surveys of massive and intermediate-mass magnetic candidates. In Section 2, we describe the photometric observations that were used and the analysis that was performed to select candidates. Section 3 describes the follow-up spectropolarimetry of four of these candidates and details the results of our magnetometric analysis. Finally, in Section 4, we discuss our results and draw conclusions about the directions our work will take moving forward.

## 2 PHOTOMETRY

### 2.1 Observations

Photometric observations were obtained by *TESS*. In the context of this mission, the sky is divided into “sectors” that are observed for 27.4 d. Most objects lie within only one sector, although there is some overlap between the sectors (especially toward the ecliptic poles) leading to some objects being observed for a longer temporal baseline.

The *TESS* bandpass is broad, covering wavelengths between about 600 and 1000 nm. While about half a billion point sources are included in the *TESS* Input Catalogue (TIC; Stassun et al. 2018, 2019) and thus appear in the 30-min cadence full-frame images (FFIs), the Candidate Target List (CTL) contains a subset of priority objects to be observed in 2-min cadence. The *TESS* Science Processing Operations Center (SPOC; Jenkins et al. 2016) releases reduced light curves based on the 2-min cadence data at the Mikulski Archive for Space Telescopes (MAST)<sup>2</sup>. While this reduction is optimized for exoplanet detection and certain stellar signals might therefore be suppressed (especially longer-duration signals in hot stars, e.g. Barron et al. 2020), it remains a useful resource for an efficient first-pass effort at identifying candidate magnetic stars.

### 2.2 Target selection

We retrieved 2-min cadence light curves from MAST for objects identified as B-type stars in the SIMBAD database that were observed by *TESS* in Sectors 1 to 6. We then performed a Lomb-Scargle frequency analysis of these light curves (Lomb 1976; Scargle 1982) and identified potential rotational modulation signals in a subset of them based on the criteria laid out by Balona (2013) and adopted by Sikora et al. (2019b): specifically, the detection of a significant peak within a range of frequency consistent with rotation, as well

as typically at least one harmonic<sup>3</sup>. A thorough literature search led to the elimination of known binaries with periods corresponding to those of the suspected rotational modulation signals (or close binaries with unknown periods, which should at the very least be followed up with spectroscopy first before being considered for spectropolarimetric follow-up), as well as known magnetic stars (and stars for which previous spectropolarimetric observations had not yielded a significant magnetic detection). Stars in crowded fields with signals of ambiguous origin were also discarded.

The final target list contained seven high-probability magnetic candidates. Out of these seven stars, four were observed with follow-up spectropolarimetry from the Canada-France-Hawaii Telescope (CFHT) during the 2019B semester. These stars are listed in Table 1, along with their putative *TESS* rotational period. Their light curves (detrended following the procedure described by Bowman et al. 2018) and the associated Lomb-Scargle periodograms are shown in Fig. 1.

## 3 SPECTROPOLARIMETRY

### 3.1 Observations

Each target was observed with ESPaDOnS (an Echelle Spectropolarimetric Device for the Observation of Stars; Donati et al. 2006) at the CFHT, as part of observing program 19BC34 (PI: David-Uraz). This instrument has a high resolving power ( $R \sim 65000$ ) and covers a wavelength range of about 3600-10000 Å. Data reduction was performed using the UPENA pipeline (Martioli et al. 2011), which is based on the LIBRE-ESPRIT reduction package (Donati et al. 1997). It yields integrated spectra (Stokes  $I$  parameter), as well as circularly polarized spectra (Stokes  $V$  parameter), which are sensitive to the Zeeman effect (Zeeman 1897), thus allowing us to detect and measure astrophysical magnetic fields.

Each complete observation consists of four subexposures, each corresponding to a different angle of the Fresnel rhombs, and their combination can produce each of the aforementioned spectra, as well as two diagnostic nulls ( $N$ ), which characterize the level of noise and allow us to identify potential spurious signals in the Stokes  $V$  spectrum. The number of observations per target and exposure times are detailed in Table 1, while the longitudinal field measurement and signal-to-noise ratio (S/N) achieved for each observation appear in Table 2. It should be noted that for two of the four observations of HD 25709, only two subexposures were obtained, which means that they are not accompanied by a diagnostic null.

### 3.2 Analysis

For each star, we obtained spectral line lists using the most up-to-date version of the Vienna Atomic Line Database (VALD3; Piskunov et al. 1995; Ryabchikova et al. 1997;

<sup>3</sup> While these criteria might appear somewhat generic, more quantitative criteria can only be derived *a posteriori*, as an increasing number of magnetic detections is accomplished, by comparing the characteristics of the magnetic population to the rest of the studied sample.

<sup>2</sup> <https://archive.stsci.edu/missions-and-data/transiting-exoplanet-survey-satellite-tess>

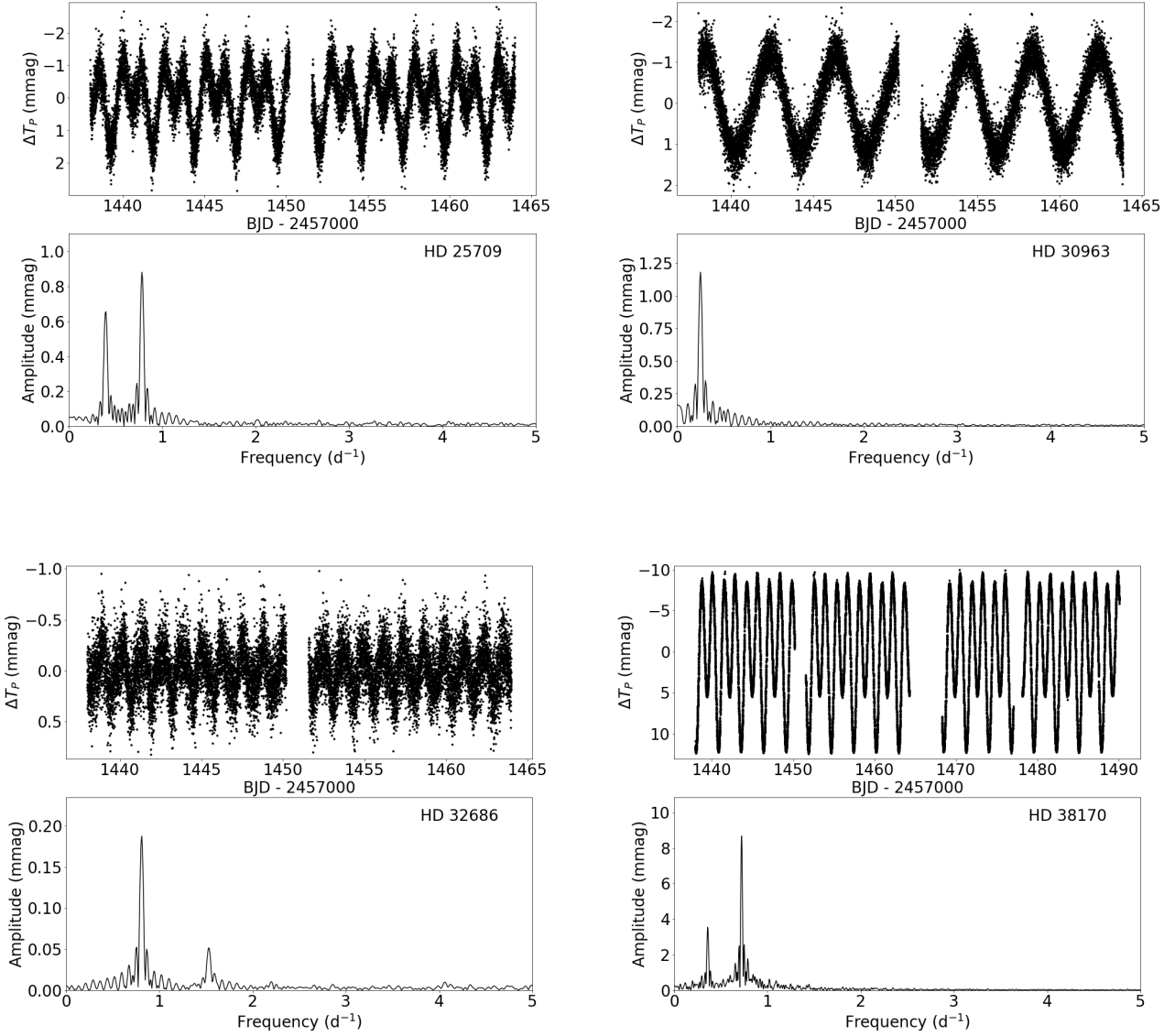


**Figure 1.** Detrended *TESS* light curves and associated Lomb-Scargle periodograms for all four targets selected for spectropolarimetric follow-up and observed by CFHT.

**Table 1.** Table of the targets and observational information. The first two columns provide identifiers, both in the HD and TIC (Stassun et al. 2019) catalogues, and the third column lists the *TESS* sectors in which each target was observed. Column 4 lists the measured fundamental (in cases where harmonics are detected) photometric period, assessed to be of rotational origin (with the uncertainty on the last digit in parentheses). Columns 5–7 list their spectral types, effective temperatures and magnitudes in the V band (with the reference for  $T_{\text{eff}}$  provided in the last column). Finally, columns 8 and 9 indicate the number of spectropolarimetric observations obtained for each star, as well as the integration time for each subexposure. It should be noted that two observations of HD 25709 consisted of only two subexposures (rather than the usual four), and can therefore not yield diagnostic nulls for comparison to their Stokes V profiles.

HD	TIC no.	Sector(s)	Period (d)	Spectral type	$T_{\text{eff}}$ (kK)	V (mag)	$N_{\text{obs}}$	$t_{\text{exp}}$ (s)	Reference ( $T_{\text{eff}}$ )
25709	34199198	5	2.554(1)	B9V	9.9	7.98	4	859	McDonald et al. (2012)
30963	9355205	5	3.9892(9)	B9III	11.5	7.23	3	318	Monier et al. (2019)
32686	213104118	5	1.2336(4)	B4II/III	14.2	6.03	2	793	Soubiran et al. (2016)
38170	140288359	5, 6	2.76618(4)	B9.5V	10.3	5.28	2	168	Hempel & Holweger (2003)

Kupka et al. 1999, 2000; Ryabchikova et al. 2015). Details about the abundances and stellar parameters used are in the following subsections. Using dedicated IDL routines, we then normalized the spectra to the continuum and constructed line masks to perform Least-Squares Deconvolution (LSD; Donati et al. 1997), a multi-line technique that increases the S/N of the Stokes  $V$  signatures upon which our magnetometric analysis is computed. Hydrogen lines were excluded, as they violate the assumption of line self-similarity required by the LSD algorithm, as well as lines severely blended with hydrogen and lines contaminated by telluric absorption.

Once the LSD profiles were computed using the iLSD method (Kochukhov et al. 2010), we calculated the disc-averaged longitudinal field using the first-order moment method (e.g. Wade et al. 2000) and we also calculated false alarm probabilities (FAPs) as discussed by Donati et al. (1997): a FAP computed on the Stokes  $V$  profile within the bounds of the LSD profile of less than  $10^{-5}$  is considered to correspond to a definite detection (DD), while a FAP between  $10^{-3}$  and  $10^{-5}$  constitutes a marginal detection (MD); anything higher is considered a non-detection (ND). Longitudinal field measurements and results of the FAP determinations are presented in Table 2.

Finally, we also perform a Bayesian analysis (as described by Petit & Wade 2012), using unconstrained rotational phases, to determine the surface field strengths that are compatible with the obtained LSD Stokes  $V$  profiles assuming an oblique global dipolar field configuration (Stibbs 1950) and marginalizing the probability density function over the geometric parameters (inclination and obliquity). The results are presented in each individual subsection below.

### 3.3 Results

#### 3.3.1 HD 25709

HD 25709 is a poorly studied object, with very few mentions in the literature. Classified as a B9V star by Houk & Swift (1999), an examination of the ESPaDOnS spectra reveals it to be an SB2 binary (see Fig. 2). Using a line list computed assuming solar abundances and the published values of  $T_{\text{eff}}$  and  $\log g$  (McDonald et al. 2012), we extracted LSD profiles for each observation with a single mask, fitting the lines to measure radial velocities and projected rotational velocities ( $v_A \sin i_A = 39.0 \pm 0.8 \text{ km s}^{-1}$ ,  $v_B \sin i_B = 19.8 \pm 0.2 \text{ km s}^{-1}$ ) for both components. We then fit a Keplerian orbit to the radial velocities, assuming that the inferred *TESS* photometric period is orbital in nature, using a Markov Chain Monte-Carlo (MCMC) sampler. The resulting radial velocity curve and its best fit, as well as the associated phased *TESS* light curve, are presented in Fig. 3.

This allows us to derive orbital and physical parameters for the system given the aforementioned assumption that the orbital period is known from *TESS* photometry ( $P_{\text{orb}} = 2.554 \text{ d}$ ); of note, this appears to be a particularly eccentric system ( $e = 0.73 \pm 0.01$ ) with a low projected total mass ( $(M_A + M_B) \sin^3 i_{\text{orb}} = 0.37 \pm 0.03 M_{\odot}$ ). Disentangling was performed on the Stokes  $I$  LSD profiles through an iterative process (Fig. 2; González & Levato 2006, as implemented by Shultz et al. 2018a,b). Stokes  $V$  was not disentangled, but the integration ranges for the magnetometric analysis were

**Table 2.** Observing log (spectropolarimetric data). For each observation, the HD number and date is provided (columns 1 and 2) as well as the peak signal-to-noise ratio (S/N) in the Stokes  $I$  spectrum, per spectral pixel (column 5). The computed longitudinal field measurement and detection status (see Section 3.2; N corresponds to a non-detection while M denotes a marginal detection and D corresponds to a definite detection) are indicated in columns 3 and 4, respectively. An asterisk next to the HD number corresponds to an observation for which only 2 subexposures were obtained; thus these observations do not have a diagnostic null. Finally, the results for HD 25709 are designated as HD 25709A (for the primary in our binary analysis) and HD 25709B (for the secondary), with the longitudinal field being measured from disentangled LSD profiles.

HD	HJD - 2 450 000	$B_z$ (G)	Detection?	S/N
25709A	8744.05269	69±51	N	552
25709A*	8804.91663	-145±161	N	248
25709A*	8806.92018	5±178	M	223
25709A	8806.98866	24±133	N	223
25709B	8744.05269	0±29	N	552
25709B*	8804.91663	12±83	N	248
25709B*	8806.92018	-46±101	N	223
25709B	8806.98866	192±75	N	223
30963	8743.13423	5±16	N	461
30963	8807.01889	-13±28	N	271
30963	8807.03561	-16±23	N	327
32686	8744.09261	21±13	N	1267
32686	8807.06450	-39±21	N	837
38170	8741.14509	-6±25	D	458
38170	8743.14585	105±14	D	685

based on the disentangled Stokes  $I$  profiles for each component, allowing us to perform a separate analysis on each component of the system.

Given the published values of parallax ( $\pi = 3.36 \pm 0.06 \text{ mas}$ ; Gaia Collaboration et al. 2018), the extinction value ( $E(B - V) = 0.01$ ) based on a comparison between the observed photometry and an interpolation of the intrinsic colours derived by Pecaut & Mamajek (2013) for a  $T_{\text{eff}}$  of 9900 K, and the associated bolometric correction ( $BC = -0.28$ ), we find the luminosity of the system to be consistent with late B-type stars. Combined with the low projected total mass, this leads to the conclusion that the inclination  $i$  is likely low, therefore the photometric variations are unlikely to be caused by eclipses. Furthermore, given the high inferred eccentricity, this system would be a good candidate to exhibit “heartbeat” variations (Thompson et al. 2012); however, the shape of the light curve does not correspond to the pattern of variability that would be expected in such a case. On the other hand, the photometric period may not be orbital after all; it is possible that the system possesses a different orbital period (which cannot currently be constrained using only four radial velocity measurements, though it must be relatively short since the radial velocity of the secondary varies by  $\sim 100 \text{ km s}^{-1}$  over two nights), and that the photometric signal is in fact linked to rotational modulation in one of the stars. Further observations (especially spectroscopy to extract new radial velocity

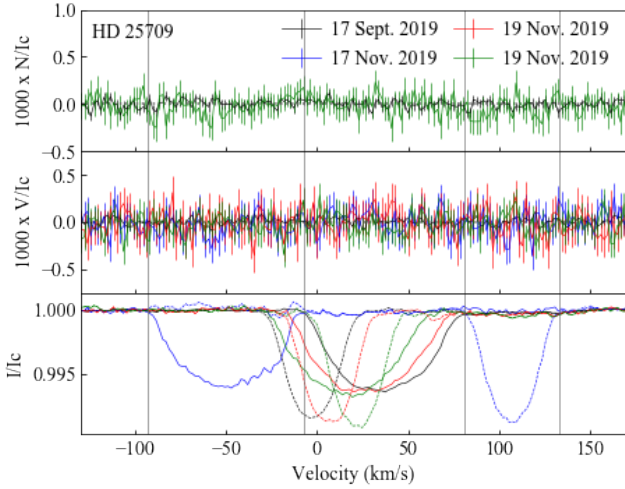


**Figure 2.** Disentangled LSD Stokes  $I$  (bottom) profiles of both components of HD 25709 (the primary is shown with a solid line, and the secondary with a dashed line), shown with the non-disentangled Stokes  $V$  profiles (middle) and the diagnostic nulls (top), for four different (colour-coded) observations (except for two diagnostic nulls which were not available). Thin vertical lines correspond to the integration ranges used for magnetometric analysis, here represented for the best separated profiles for each component. All Stokes  $V$  profiles are consistent with non-detections, while the Stokes  $I$  profiles obviously show the SB2 nature of this system.

measurements) are required to better understand this system, but such an undertaking falls outside the scope of this current study.

As for the magnetometric analysis, all disentangled profiles led to non-detections (with a smallest  $1\sigma$  error bar on  $B_z$  of 51 G for the primary and 29 G for the secondary) with one exception (for which  $\text{FAP} = 1.92 \times 10^{-4}$ ). While this would normally be considered as a marginal detection, we note that it occurs in one of the observations for which there is no diagnostic null. Therefore, this result should be viewed as inconclusive. Additionally, none of the associated longitudinal field measurements is significant at the  $3\sigma$  level.

Finally, applying the Bayesian analysis of [Petit & Wade \(2012\)](#) to the two observations consisting of full spectropolarimetric sequences (four sub-exposures), we find upper limits on the polar strength of the dipole field ( $B_{d, \text{max}}$ ) of 408 G for the primary and 244 G for the secondary (corresponding to the 95.4 per cent credible region of the probability density function, marginalized for the field strength).

### 3.3.2 HD 30963

A late B-type star, HD 30963 has not been extensively studied in the past, and was not known to be chemically peculiar at the time of our spectropolarimetric follow-up proposal. In the intervening time however, an abundance analysis based on high-resolution spectra revealed it to be a HgMn star ([Monier et al. 2019](#)). So far, no strong, globally organized magnetic field has yet been detected at the surface of such an object ([Kochukhov et al. 2013](#)). Nevertheless, we computed a line mask using the abundances and atmospheric

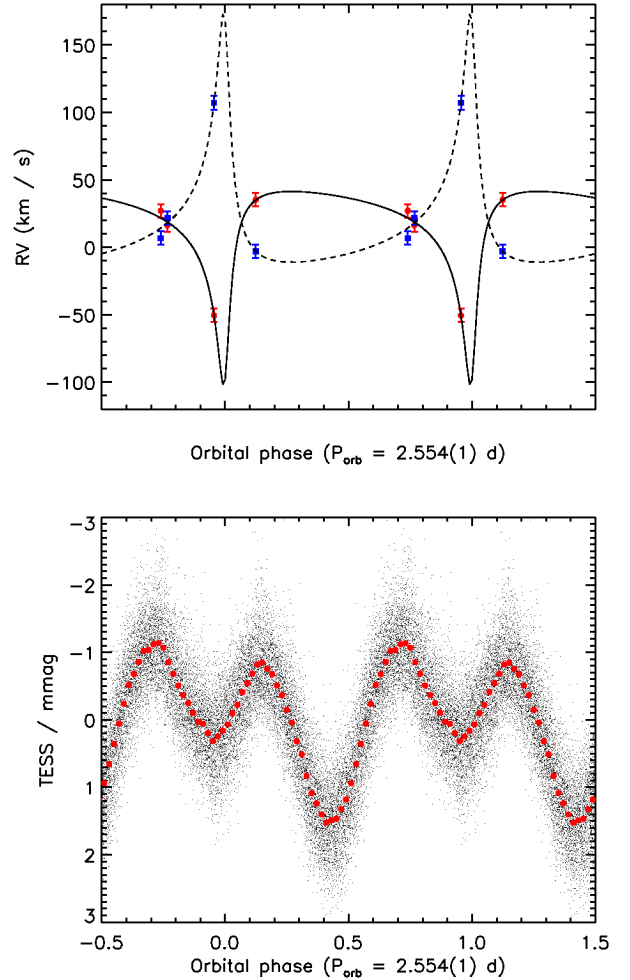


**Figure 3.** Phased radial velocity (RV) curve (top) and light curve (bottom). In the top panel, RV measurements of the primary are shown in red (with the best fit represented by a solid black line), while measurements of the secondary are shown in blue (with a dashed curve to represent the best fit). In the bottom panel, red dots represent observations binned in phase.

parameters of [Monier et al. \(2019\)](#) and performed our magnetometric analysis (our LSD profiles are shown in Fig. 4). This resulted in non-detections (with a smallest error bar on the longitudinal field of 16 G; Table 2). Our Bayesian analysis yields in turn an upper limit of  $B_{d, \text{max}} = 63$  G (95.4 per cent credible region). Nevertheless, we evaluate that it is probable that the signal recovered by *TESS* is rotational in origin, as has been observed in similar objects (e.g. [Prvák et al. 2020](#)).

### 3.3.3 HD 32686

Classified as a B4II/III by [Houk & Swift \(1999\)](#), HD 32686 is a fairly evolved star presumably approaching the end of its main sequence lifetime. It has not previously been noted to exhibit chemical peculiarities, and it should be noted that it does not show an excess in  $\Delta a$  photometry ([Vogt et al. 1998](#)), therefore we adopted solar abundances, together with the at-

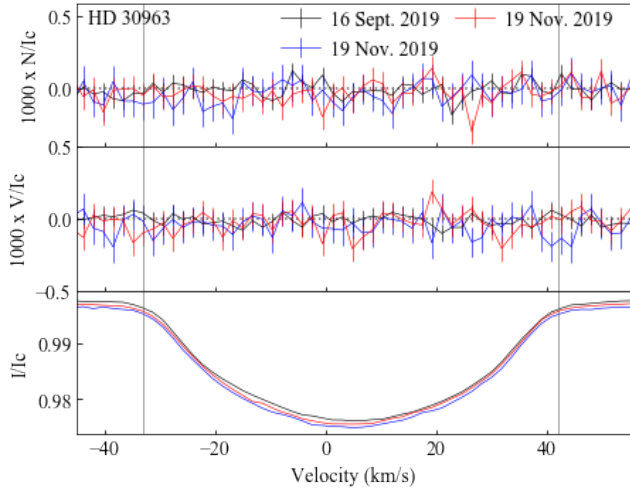


**Figure 4.** LSD profiles of HD 30963 in Stokes  $I$  (bottom),  $V$  (middle) and the diagnostic nulls (top), for three different observations (colour-coded). The integration range used for magneto-metric analysis is represented by thin vertical lines. All Stokes  $V$  profiles are consistent with non-detections.

mospheric parameters tabulated by [Soubiran et al. \(2016\)](#), to compute a VALD3 line list to use in our magnetometric analysis. This resulted in non-detections, with a best longitudinal field error bar of 23 G. However, apparent line profile variations (Fig. 5) between the two observations, combined with anomalously strong helium lines, led us to the suspicion that this might be a chemically peculiar star nonetheless. While a detailed abundance analysis is outside the scope of this study, we tested a line mask previously computed for a Bp star of similar effective temperature (HD 145501C; [Netopil et al. 2017](#)), which yielded more stringent constraints on the longitudinal field due to the increased number of lines, lowering the error bar to 13 G. These results are the ones presented in Table 2 (and they are still non-detections). We also based our Bayesian analysis on the LSD profiles yielded by the second mask, which leads to an upper limit of  $B_{d, \max} = 140$  G (95.4 per cent credible region).

It should be noted that this non-detection might not be entirely surprising given the apparent evolutionary stage of HD 32686. Under the assumption of flux conservation, typical dipolar fields observed in main sequence stars might weaken from a few kG to a few tens of G near the terminal age main-sequence (e.g. [Keszthelyi et al. 2019](#)), just below the magnetic sensitivity achieved in this study. Interestingly, this star also exhibits the weakest photometric variations of the four stars that were observed. This could potentially hint at the presence of a very weak field on the surface of HD 32686, below our current detection limits, although there is no demonstrated correlation between field strength and the amplitude of rotationally modulated light-curve variability in magnetic B-type stars. That said, its relatively short rotation period ( $\sim 1.23$  d) is somewhat surprising in that regard, as a magnetic star would surely have undergone a significant amount of magnetic braking over its lifetime (e.g. [ud-Doula et al. 2009](#)).

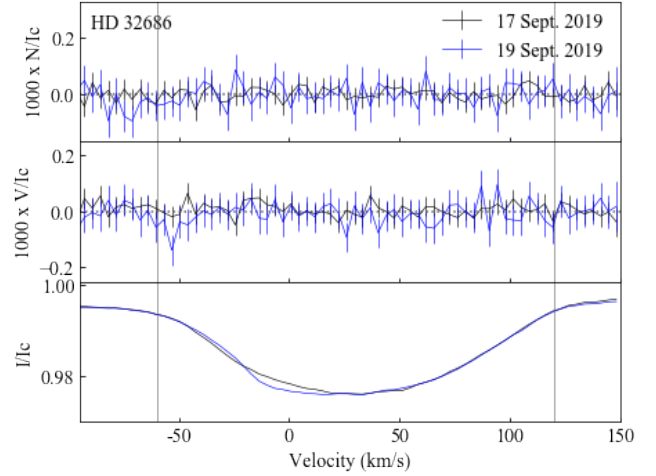


**Figure 5.** Same as Fig. 4, but for HD 32686; note that there appear to be slight variations in the Stokes  $I$  line profile.

### 3.3.4 HD 38170

Although it is not listed as being chemically peculiar in the [Renson & Manfroid \(2009\)](#) catalog, HD 38170 (= WZ Col) was found to be overabundant in strontium and barium by [Hempel & Holweger \(2003\)](#) and identified as a probable  $\alpha^2$  CVn variable by [Dubath et al. \(2011\)](#) based on Hipparcos photometry ( $P = 1.38$  d; we infer a period twice as long from the *TESS* light curve). It also shows a strong excess in  $\Delta\alpha$  photometry ([Vogt et al. 1998](#)), further confirming its status as a chemically peculiar star. Moreover, as the brightest star in our sample, HD 38170 thus represented *a priori* the most promising candidate to detect a magnetic field among the four objects which form this study.

We constructed our line mask using the abundances derived by [Hempel & Holweger \(2003\)](#), as well as non-solar abundances for chromium and rare-Earth elements, based on their apparent temperature dependence in ApBp stars<sup>4</sup> ([Ryabchikova & Romanovskaya 2017](#)). Both observations yielded a definite detection (based on the FAPs) and the longitudinal field measured from the second observation constitutes a  $7.5\sigma$  detection ( $B_z = 105 \pm 14$  G). The associated LSD profiles are shown in Fig. 6, and a clear signal can be seen in Stokes  $V$ . As a result, we conclude that this star constitutes a firm new magnetic detection.

Using the Gaia parallax ( $\pi = 8.90 \pm 0.15$  mas; [Gaia Collaboration et al. 2018](#)), expected intrinsic colour ( $B - V = -0.04$ ; [Pecaut & Mamajek 2013](#)) and bolometric correction (accounting for its chemical peculiarity,  $BC = -0.21$ ; [Netopil et al. 2008](#)) for this star, we derive its stellar parameters using the MCMC sampler described by [Shultz et al. \(2019a\)](#). The results are listed in Table 3. Based on the obtained radius and the measured value of  $v \sin i$  ( $57 \pm 5$  km s<sup>-1</sup>), as well as the period determined from the *TESS* light curve (assumed to be rotationally modulated), we can also constrain the inclination  $i$ . It is included in Table 3.

Finally, we performed a Bayesian analysis on our LSD

<sup>4</sup> We used nominal values of  $\log([\text{Cr}/\text{H}]) = -4.0$ ,  $\log([\text{Pr}/\text{H}]) = \log([\text{Nd}/\text{H}]) = \log([\text{Eu}/\text{H}]) = \log([\text{Ce}/\text{H}]) = -8.0$ .

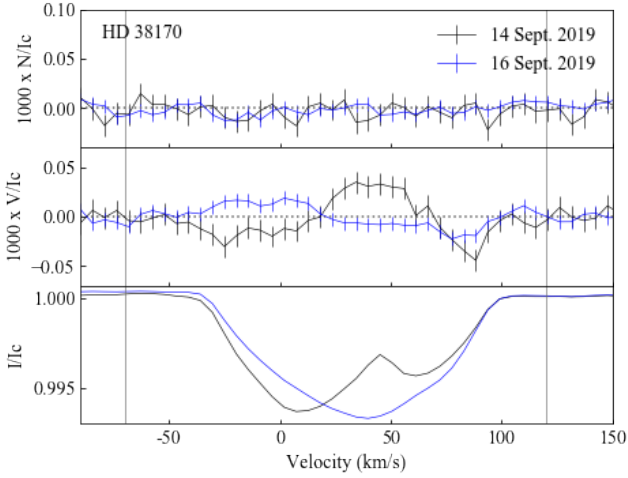


**Figure 6.** Same as Fig. 4, but for HD 38170. Notice the asymmetry in the black Stokes  $I$  profile, consistent with the presence of chemical spots on the surface of the star. Both Stokes  $V$  profiles are consistent with a definite magnetic detection.

**Table 3.** Stellar parameters of HD 38170, fit with an MCMC sampler, in order: luminosity, surface gravity (in cgs units), polar radius, mass, age (based on the evolutionary tracks of Ekström et al. 2012), fractional main-sequence age and inclination of the rotational axis with respect to the line of sight.

Stellar parameters	
$\log L$	$2.0 \pm 0.1$
$\log g$	$3.86 \pm 0.06$
$R_p$ ( $R_\odot$ )	$3.3 \pm 0.3$
$M_*$ ( $M_\odot$ )	$2.8 \pm 0.1$
Age (Myr)	$394^{+10}_{-17}$
$t/t_{\text{TAMS}}$	$0.68^{+0.07}_{-0.04}$
$i$ ( $^\circ$ )	$67 \pm 6$

profiles, yielding a dipolar field strength of  $B_d = 254^{+78}_{-49}$  G (with a 68.3 per cent credible region). We note that our modelling assumes a Voigt line profile in Stokes  $I$ , consistent with stellar rotation. Therefore, the line profile variability that is evident in the Stokes  $I$  profiles of HD 38170 is not taken into account, but we consider this to be a reasonable approach given the fact that we reproduce the general shape of the Stokes  $V$  profiles satisfactorily nonetheless.

The fairly weak dipolar field strength that we obtain is consistent with the moderately high fractional main-sequence age, assuming flux conservation. The model with the maximum *a posteriori* probability yielded values of  $B_d = 257$  G,  $i = 57^\circ$  and  $\beta = 60^\circ$ , with a difference in rotational phase of  $\Delta\phi = 0.7222$ , which is almost identical to what we obtain given the *TESS* photometric period (0.7233). We note that the value of the inclination falls just a bit outside of the range obtained from the stellar parameter analysis; marginalizing the two-dimensional posterior probability density function between the inclination and obliquity for values of  $i$  located within that range, we find that  $\beta = 45^{+10}_{-5}$ . While this preliminary work seems to indicate that

a dipolar model can explain some of the characteristics of our observations pretty well, more observations and sophisticated modelling (such as Zeeman Doppler Imaging or ZDI; Semel 1989) would be required for a full magnetic characterization of this star. Such an endeavour, however, falls outside the scope of our current study.

#### 4 CONCLUSIONS AND DISCUSSION

Out of four B-type stars that were selected photometrically to exhibit rotational modulation from the *TESS* mission, one was found to host a detectable magnetic field. We placed upper limits on the magnetic field strength inferred from the non-detections. A previously unknown binary system (HD 25709) was also found. The detection was achieved for HD 38170, which apparently is an evolved late B-type star. The fairly weak inferred field strength ( $B_d \sim 250$  G) is compatible with its proposed evolutionary status, and therefore this new detection lies in an undersampled region of the Hertzsprung-Russell diagram (e.g. Petit & David-Uraz 2020), given the dearth of known evolved magnetic massive stars (Fossati et al. 2016).

While our detection rate of 25 per cent is significantly higher than the observed incidence of magnetic OBA stars, it is still lower than the detection rate that we aim to achieve with our larger targeted survey ( $> 50$  per cent). However, we do not consider it to be representative of the potential of *TESS* data to select magnetic candidates, because of the extremely small number statistics. That said, the results of this preliminary study do emphasize certain criteria that must be applied, beyond the possible detection of rotational modulation in a light curve. In particular, the following types of targets should not be considered for spectropolarimetric follow-up in the context of our targeted survey:

- binary (or multiple) stars with orbital periods compatible with the periods extracted from the photometry, or with unknown orbital periods; we would argue against removing binaries with a known orbital period that is different from the one that is recovered from their light curve, as magnetic OBA stars in binaries (and especially close binaries) are of particular interest (Alecian et al. 2015);
- HgMn stars, which systematically do not show evidence of strong, globally organized fields<sup>5</sup> despite occasionally exhibiting rotationally modulated photometric signals, as well as classical Be stars, for which no magnetic field has been detected to date (Wade et al. 2016b), as such a field would potentially disrupt a Keplerian disc (ud-Doula et al. 2018);
- objects whose light curves only show very low amplitude variations (such as HD 32686), since although these variations might still be due to magnetism, there is a higher likelihood overall that they might be caused by, e.g., contamination in a crowded field than in cases with higher amplitudes (although this criterion should perhaps not be applied to O stars, as magnetospheric scattering might lead

<sup>5</sup> Dedicated efforts to achieve high precision magnetometric measurements of these objects remain warranted, as the origin of their chemical peculiarities is still unknown and hypothesized to be related to magnetism, but they fall outside the scope of our larger targeted survey.

to smaller variations than photospheric spots; Munoz et al. 2020).

While the number of stars involved precludes an efficient use of machine learning methods, future detections will nonetheless help us to iteratively improve our candidate selection criteria. This will lead to a high-yield survey and ultimately better statistics for the population of massive and intermediate-mass magnetic stars.

## ACKNOWLEDGEMENTS

This paper includes data collected by the *TESS* mission. Funding for the *TESS* mission is provided by the NASA Explorer Program. Funding for the *TESS* Asteroseismic Science Operations Centre is provided by the Danish National Research Foundation (Grant agreement no.: D NRF106), ESA PRODEX (PEA 4000119301) and Stellar Astrophysics Centre (SAC) at Aarhus University. We thank the *TESS* and TASC/TASOC teams for their support of the present work. This research has made use of the SIMBAD database, operated at CDS, Strasbourg, France. Some of the data presented in this paper were obtained from the Mikulski Archive for Space Telescopes (MAST). STScI is operated by the Association of Universities for Research in Astronomy, Inc., under NASA contract NAS5-2655. This work has made use of the VALD database, operated at Uppsala University, the Institute of Astronomy RAS in Moscow, and the University of Vienna.

ADU and GAW acknowledge the support of the Natural Science and Engineering Research Council of Canada (NSERC). MES acknowledges the financial support provided by the Annie Jump Cannon Fellowship, supported by the University of Delaware and endowed by the Mount Cuba Astronomical Observatory. VP acknowledges support from the National Science Foundation under Grant No. 1747658. The research leading to these results has received funding from the European Research Council (ERC) under the European Unions Horizon 2020 research and innovation programme (grant agreement No. 670519: MAMSIE).

Finally, the authors also thank Z. Keszthelyi, J. Krtićka, A. F. J. Moffat, E. Paunzen and E. Semenko for their helpful comments.

## REFERENCES

- Alecian E., et al., 2015, in Meynet G., Georgy C., Groh J., Stee P., eds, IAU Symposium Vol. 307, New Windows on Massive Stars. pp 330–335 ([arXiv:1409.1094](https://arxiv.org/abs/1409.1094)), [doi:10.1017/S1743921314007030](https://doi.org/10.1017/S1743921314007030)
- Babcock H. W., 1958, *ApJ*, **128**, 228
- Bagnulo S., et al., 2020, arXiv e-prints, [p. arXiv:2002.12061](https://arxiv.org/abs/2002.12061)
- Balona L. A., 2013, *MNRAS*, **431**, 2240
- Barron J., Wade G. A., Bowman D. M., David-Uraz A., Munoz M. S., Pablo H., Simón-Díaz S., 2020, arXiv e-prints, [p. arXiv:2001.04534](https://arxiv.org/abs/2001.04534)
- Bowman D. M., Buyschaert B., Neiner C., Pápics P. I., Oksala M. E., Aerts C., 2018, *A&A*, **616**, A77
- Buyschaert B., Neiner C., Martin A. J., Aerts C., Bowman D. M., Oksala M. E., Van Reeth T., 2018, *MNRAS*, **478**, 2777
- David-Uraz A., et al., 2019, *MNRAS*, **487**, 304
- Donati J. F., Landstreet J. D., 2009, *ARA&A*, **47**, 333
- Donati J. F., Semel M., Carter B. D., Rees D. E., Collier Cameron A., 1997, *MNRAS*, **291**, 658
- Donati J. F., Catala C., Landstreet J. D., Petit P., 2006, ES-PaDONs: The New Generation Stellar Spectro-Polarimeter. Performances and First Results. p. 362
- Dubath P., et al., 2011, *MNRAS*, **414**, 2602
- Eikenberry S. S., et al., 2014, *ApJ*, **784**, L30
- Ekström S., et al., 2012, *A&A*, **537**, A146
- Fossati L., et al., 2016, *A&A*, **592**, A84
- Gaia Collaboration et al., 2018, *A&A*, **616**, A1
- González J. F., Levato H., 2006, *A&A*, **448**, 283
- Grunhut J. H., et al., 2017, *MNRAS*, **465**, 2432
- Hempel M., Holweger H., 2003, *A&A*, **408**, 1065
- Houk N., Swift C., 1999, Michigan Spectral Survey, **5**, 0
- Jenkins J. M., et al., 2016, The *TESS* science processing operations center. p. 99133E, [doi:10.1117/12.2233418](https://doi.org/10.1117/12.2233418)
- Keszthelyi Z., Meynet G., Georgy C., Wade G. A., Petit V., David-Uraz A., 2019, *MNRAS*, **485**, 5843
- Kochukhov O., Makaganiuk V., Piskunov N., 2010, *A&A*, **524**, A5
- Kochukhov O., et al., 2013, *A&A*, **554**, A61
- Kupka F., Piskunov N., Ryabchikova T. A., Stempels H. C., Weiss W. W., 1999, *A&AS*, **138**, 119
- Kupka F. G., Ryabchikova T. A., Piskunov N. E., Stempels H. C., Weiss W. W., 2000, *Baltic Astronomy*, **9**, 590
- Landstreet J. D., Bagnulo S., Andretta V., Fossati L., Mason E., Silaj J., Wade G. A., 2007, *A&A*, **470**, 685
- Landstreet J. D., et al., 2008, *A&A*, **481**, 465
- Lomb N. R., 1976, *Ap&SS*, **39**, 447
- Martio E., Teeple D., Manset N., 2011, in Gajadhar S., et al., eds, Telescopes from Afar. p. 63
- McDonald I., Zijlstra A. A., Boyer M. L., 2012, *MNRAS*, **427**, 343
- Monier R., Griffin E., Gebran M., Kılıçoğlu T., Merle T., Royer F., 2019, *AJ*, **158**, 157
- Munoz M. S., Wade G. A., Nazé Y., Puls J., Bagnulo S., Szymański M. K., 2020, *MNRAS*, **492**, 1199
- Netopil M., Paunzen E., Maitzen H. M., North P., Hubrig S., 2008, *A&A*, **491**, 545
- Netopil M., Paunzen E., Hümmelich S., Bernhard K., 2017, *MNRAS*, **468**, 2745
- Pecaút M. J., Mamajek E. E., 2013, *ApJS*, **208**, 9
- Petit V., David-Uraz A., 2020, arXiv e-prints, [p. arXiv:2004.04241](https://arxiv.org/abs/2004.04241)
- Petit V., Wade G. A., 2012, *MNRAS*, **420**, 773
- Petit V., et al., 2013, *MNRAS*, **429**, 398
- Piskunov N. E., Kupka F., Ryabchikova T. A., Weiss W. W., Jeffery C. S., 1995, *A&AS*, **112**, 525
- Prvák M., Krtićka J., Korhonen H., 2020, *MNRAS*, **492**, 1834
- Renson P., Manfroid J., 2009, *A&A*, **498**, 961
- Ricker G. R., et al., 2015, *Journal of Astronomical Telescopes, Instruments, and Systems*, **1**, 014003
- Ryabchikova T. A., Romanovskaya A. M., 2017, *Astronomy Letters*, **43**, 252
- Ryabchikova T. A., Piskunov N. E., Kupka F., Weiss W. W., 1997, *Baltic Astronomy*, **6**, 244
- Ryabchikova T., Piskunov N., Kurucz R. L., Stempels H. C., Heiter U., Pakhomov Y., Barklem P. S., 2015, *Phys. Scr.*, **90**, 054005
- Scargle J. D., 1982, *ApJ*, **263**, 835
- Schneider F. R. N., Podsiadlowski P., Langer N., Castro N., Fossati L., 2016, *MNRAS*, **457**, 2355
- Schöller M., et al., 2017, *A&A*, **599**, A66
- Semel M., 1989, *A&A*, **225**, 456
- Shultz M., Rivinius T., Wade G. A., Alecian E., Petit V., BinaM-IcS Collaboration 2018a, *MNRAS*, **475**, 839
- Shultz M. E., et al., 2018b, *MNRAS*, **475**, 5144
- Shultz M. E., et al., 2019a, *MNRAS*, **485**, 1508
- Shultz M. E., et al., 2019b, *MNRAS*, **490**, 274

- Sikora J., Wade G. A., Power J., Neiner C., 2019a, *MNRAS*, **483**, 3127
- Sikora J., et al., 2019b, *MNRAS*, **487**, 4695
- Soubiran C., Le Campion J.-F., Brouillet N., Chemin L., 2016, *A&A*, **591**, A118
- Stassun K. G., et al., 2018, *AJ*, **156**, 102
- Stassun K. G., et al., 2019, *AJ*, **158**, 138
- Stibbs D. W. N., 1950, *MNRAS*, **110**, 395
- Thompson S. E., et al., 2012, *ApJ*, **753**, 86
- Villebrun F., et al., 2019, *A&A*, **622**, A72
- Vogt N., Kerschbaum F., Maitzen H. M., Faundez-Abans M., 1998, *A&AS*, **130**, 455
- Wade G. A., Donati J. F., Landstreet J. D., Shorlin S. L. S., 2000, *MNRAS*, **313**, 851
- Wade G. A., et al., 2016a, *MNRAS*, **456**, 2
- Wade G. A., Petit V., Grunhut J. H., Neiner C., MiMeS Collaboration 2016b, Magnetic Fields of Be Stars: Preliminary Results from a Hybrid Analysis of the MiMeS Sample. p. 207
- Walborn N. R., 1972, *AJ*, **77**, 312
- Walborn N. R., 1974, *ApJ*, **191**, L95
- Zeeman P., 1897, *ApJ*, **5**, 332
- ud-Doula A., Owocki S. P., Townsend R. H. D., 2009, *MNRAS*, **392**, 1022
- ud-Doula A., Owocki S. P., Kee N. D., 2018, *MNRAS*, **478**, 3049

This paper has been typeset from a  $\text{\TeX}/\text{\LaTeX}$  file prepared by the author.